Acta Crystallographica Section F
Structural Biology and Crystallization Communications
ISSN 1744-3091

Cloning, expression, purification, crystallization and preliminary X-ray diffraction analysis of the regulatory domain of aspartokinase (Rv3709c) from *Mycobacterium tuberculosis*

Linda Schuldt,*‡ Ruth Suchowersky, Katharina Veith,§ Jochen Mueller-Dieckmann and Manfred S. Weiss¶

EMBL Hamburg Outstation, c/o DESY, Notkestrasse 85, D-22603 Hamburg, Germany

‡ Present address: PUMPKIN – Centre for Membrane Pumps in Cells and Disease, Department of Molecular Biology, Aarhus University, Gustav Wieds Vej 10c, DK-8000 Aarhus C, Denmark.
§ Present address: Max-Planck-Institute for Developmental Biology, Spemannstrasse 35, Department II – Biochemistry, D-72076 Tübingen, Germany.
¶ Present address: Helmholtz-Zentrum Berlin für Materialien und Energie, Macromolecular Crystallography (BESSY-MX), Albert-Einstein-Strasse 15, D-12489 Berlin, Germany.

Correspondence e-mail: lschuldt@mb.au.dk

Received 23 November 2010
Accepted 3 January 2011

The regulatory domain of *Mycobacterium tuberculosis* aspartokinase (*Mtb*-AK, *Mtb*-Ask, Rv3709c) has been cloned, heterologously expressed in *Escherichia coli* and purified using standard chromatographic techniques. Screening for initial crystallization conditions using the regulatory domain (AK-β) in the presence of the potential feedback inhibitor threonine identified four conditions which yielded crystals suitable for X-ray diffraction analysis. From these four conditions five different crystal forms of *Mtb*-AK-β resulted, three of which belonged to the orthorhombic system, one to the tetragonal system and one to the monoclinic system. The highest resolution (1.6 Å) was observed for a crystal form belonging to space group $P2_12_12_1$, with unit-cell parameters a = 53.70, b = 63.43, c = 108.85 Å and two molecules per asymmetric unit.

1. Introduction

Tuberculosis (TB) is an airborne bacterial disease that newly infects nearly ten million individuals worldwide every year. TB causes 2–3 million deaths per annum, making it the disease with the highest death rate of all infectious bacterial diseases (World Health Organization, 2009). As a consequence, TB was declared a global health emergency by the World Health Organization in 1993. The pathogen that is predominantly responsible for causing TB is *Mycobacterium tuberculosis* (*Mtb*). First-line drugs for the treatment of TB such as isoniazid, rifampin, ethambutol and streptomycin were introduced in the 1950s and 1960s. However, owing to poor patient compliance and the misuse of antibiotics, the number of multidrug-resistant (MDR) and even extensively drug-resistant (XDR) *Mtb* strains is constantly increasing. This represents a serious threat to global TB control (Raviglione & Smith, 2007). Therefore, a need for new antibacterial drugs is evident. New drug targets may be found in biosynthetic pathways that are critical for the survival of the pathogen but do not exist in humans. The lysine-biosynthetic pathway fulfils these criteria (Hutton *et al.*, 2007): the end product L-lysine is required for protein production and its direct precursor *meso*-diaminopimelate (*meso*-DAP) plays a crucial role in cell-wall stability (Pavelka & Jacobs, 1996).

The first step in the biosynthesis of the aspartic acid group amino acids lysine, threonine and methionine is catalyzed by the enzyme aspartokinase (AK, Ask, DapG; EC 2.7.2.4; Black & Wright, 1955; Cole *et al.*, 1998). The side-chain carboxyl group of L-aspartate is phosphorylated using ATP to form the energetically activated L-4-aspartylphosphate (Fig. 1; Umbarger, 1978). Similar to other enzymes involved in the biosynthesis of amino acids, AK can be feedback-

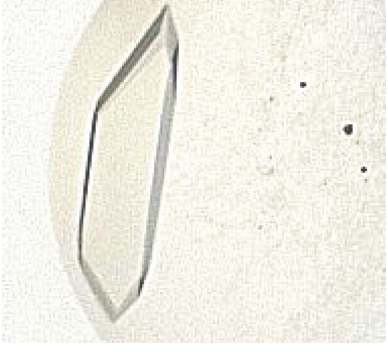

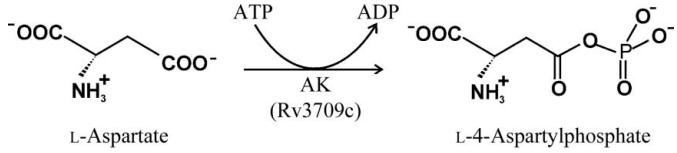

Figure 1
Schematic representation of the reaction scheme of the $\alpha_2\beta_2$-type aspartokinase from *Mtb*.

inhibited by the end products of the pathway. Organisms may either have a single isoform or possess multiple isoforms of AK. When several isoforms of AK are present it is often observed that each isoform is controlled individually. This is the case in Gram-negative bacteria such as, for instance, *Escherichia coli* (Faehnle *et al.*, 2006). When only one AK isoform exists multivalent control of the enzymatic activity is often observed. This requires the presence of more than one binding site for the various feedback inhibitors. *Mtb* exhibits a single isoform, but no information about potential feedback inhibitors has been described in the literature to date. Based on sequence comparisons, it may be speculated that both threonine and lysine are able to act as potential feedback inhibitors.

All monofunctional AKs examined to date have been found to be built up of an N-terminal amino-acid kinase domain followed by a regulatory domain, which in turn is built up of a variable number of ACT domains [where ACT stands for **A**spartate kinase/**C**horismate mutase/**T**yrA (prephenate dehydrogenase)]. Based on the resulting architecture, three classes of AKs exist (Robin *et al.*, 2010). Homo-oligomeric AKs possess identical subunits and can be further divided into AKs which possess two (class I) or four (class III) ACT domains. Heterotetrameric AKs (class II) contain equal numbers of α- and β-subunits, resulting in $\alpha_2\beta_2$-type aspartokinases in which each chain contains two ACT domains. The α- and β-subunits are encoded by in-frame overlapping genes. In addition to monofunctional AKs, bifunctional enzymes which possess aspartokinase and homoserine dehydrogenase activity also exist (Cohen *et al.*, 1969). *Mtb* has a single gene within its genome which is assigned as a monofunctional $\alpha_2\beta_2$-type aspartokinase encoded by open-reading frame Rv3709c. The resulting polypeptide chain of the AK α-subunit (AK-α) contains all residues 1–421. The AK β-subunit (AK-β) is missing the first 249 amino-acid residues (Fig. 2) and consists of residues 250–421. The catalytic domain is built up by the N-terminal part of the AK-α subunit. The regulatory domain of *Mtb*-AK comprises the C-terminal part of AK-α and the complete AK-β subunit. To simplify the discussion in this work, the regulatory domain will be denoted as being built up of two AK-β subunits.

At present, no structural information is available on a mycobacterial AK. Recently, the X-ray structure of the full-length $\alpha_2\beta_2$-type AK from *Corynebacterium glutamicum* was described (PDB entries 3aaw, 3ab2 and 3ab4; Yoshida *et al.*, 2010). In addition, structural information on the regulatory domain of $\alpha_2\beta_2$-type AKs is available for *C. glutamicum* (PDB entry 2dtj; Yoshida *et al.*, 2007), *Thermus thermophilus* (PDB entries 2zho and 2dt9; Yoshida *et al.*, 2009) and *Neisseria meningitides* (PDB entry 2re1; C. Chang, H. Li, M. Gu & A. Joachimiak, unpublished work). These domains share 68, 37 and 38% sequence identity with *Mtb*-AK-β, respectively. In all cases AK-β was found to be dimeric in the crystal, with each subunit harbouring two conserved ACT domains. ACT domains are widespread in nature and are for instance also found in other allosteric enzymes involved in amino-acid and purine biosynthesis (Chipman & Shaanan, 2001).

In this report, we describe the cloning of *Mtb*-AK-β (Rv3709c) from genomic DNA, the heterologous overexpression of the protein in *E. coli*, its purification to homogeneity and its successful crystallization. As part of a long-term effort to structurally characterize all of the enzymes of the lysine-biosynthetic pathway in *Mtb*, diffraction-quality crystals and structures have already been obtained for the enzymes *Mtb*-Asd (Vyas *et al.*, 2008), *Mtb*-DapA (Kefala & Weiss, 2006, 2008), *Mtb*-DapB (Kefala, Janowski *et al.*, 2005; Janowski *et al.*, 2010), *Mtb*-DapD (Schuldt *et al.*, 2008, 2009), *Mtb*-DapC (Weyand *et al.*, 2006, 2007) and *Mtb*-LysA (Kefala, Perry *et al.*, 2005; Weyand *et al.*, 2009). In addition, the structure of *Mtb*-DapF has recently been described by Usha *et al.* (2009). Hence, *Mtb*-AK-β represents the eighth lysine-biosynthetic enzyme for which diffracting crystals have been obtained, making lysine biosynthesis in *M. tuberculosis* one of the best characterized pathways in this organism to date.

2. Experimental methods

2.1. Cloning

The regulatory domain of *Mtb*-AK (residues 250–421 of Rv3709c) was cloned from genomic DNA into the expression vector pETM-13. The forward primer for AK-β was 5′-CCTT*CATGAG*CGAAGAC-CCCATCCTGAC-3′ containing a *Bsp*HI restriction site (in italics). The reverse primer 5′-CCT*CTCGAG*CCGTCCCGTCCCC-3′ contained an *Xho*I restriction site (in italics). The digested insert was cloned into an *Nco*I/*Xho*I-digested pETM-13 vector. Correct cloning was confirmed by sequencing. The finally produced *Mtb*-AK-β protein possesses the additional residues MS and LEHHHHHH at the N- and C-termini, respectively, exhibiting a molecular mass of 19 340 Da and an extinction coefficient of 4470 M^{-1} cm^{-1} as calculated using the *ProtParam* web service (Gasteiger *et al.*, 2005).

2.2. Expression and purification

The recombinant plasmid was used to transform *E. coli* BL21 Star (DE3) cells coexpressing chaperone combination 2 (DeMarco *et al.*, 2007). Cells from a 7.5 ml overnight culture were used for the inoculation of 750 ml LB broth medium containing spectinomycin (50 µg ml^{-1}), chloramphenicol (17 µg ml^{-1}) and kanamycin (50 µg ml^{-1}). Cells were grown at 310 K and 190 rev min^{-1} until an $OD_{600\,nm}$ of 0.6–0.8 was reached. Protein expression was induced using 300 µ*M* isopropyl β-D-1-thiogalactopyranoside (IPTG). Cells were harvested by centrifugation 3 h after induction. All cell pellets were stored at 253 K until further processing.

1–2 g of wet cell pellet was dissolved in 10 ml buffer *A* [100 m*M* bis-Tris pH 6.0, 200 m*M* NaCl, 20 m*M* imidazole, 5 m*M* β-mercaptoethanol (β-ME)] supplemented with one Complete Mini EDTA-free Protease Inhibitor Cocktail tablet (Roche) per 20 ml and

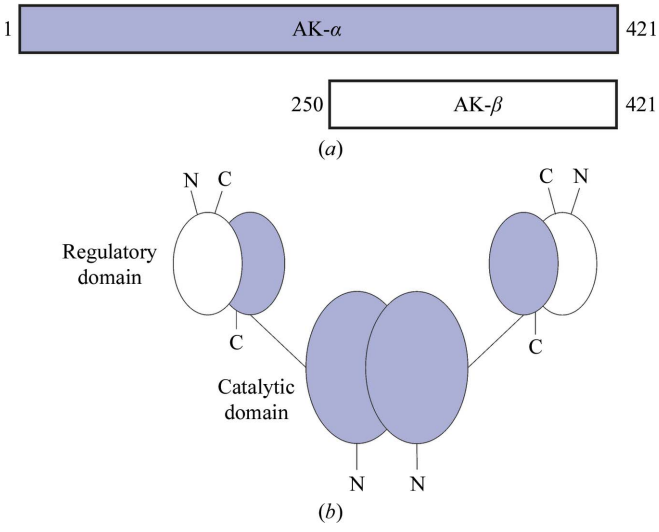

Figure 2
Architecture of *Mtb*-AK. (*a*) The overlapping polypeptide chains of the AK α-subunit (purple) and β-subunit (white) are indicated. (*b*) The $\alpha_2\beta_2$-type AK domain organization is shown. The N-terminal region of AK-α forms the catalytic domain. The C-terminal part of the AK-α subunits and two AK-β subunits make up two separated regulatory domains.

lysed by sonication three times for 3 min using 0.4 s pulses at 277 K. The cell debris was pelleted by centrifugation for 60 min at 277 K and 43 000*g*. The crude lysate was filtered through a 0.22 µm Millex GP filter unit (Millipore). For affinity chromatography, 2 ml Ni^{2+}-NTA beads (Qiagen) in a 12 cm Econo-Pac Chromatography column (Bio-Rad) were pre-equilibrated with buffer *A*. The cell lysate was loaded onto the affinity column. In order to remove unbound protein, the column was washed with 20 ml buffer *A*. The protein was eluted with a step gradient of buffer *B* (100 m*M* bis-Tris pH 6.0, 200 m*M* NaCl, 400 m*M* imidazole, 5 m*M* β-ME) immediately before proceeding to the next purification step. The protein solution was adjusted to a total volume of 5 ml and filtered through a 0.22 µm Millex GP filter unit (Millipore). Subsequently, the protein was purified by size-exclusion chromatography using a Superdex S75 16/60 column (GE Healthcare) which was pre-equilibrated with buffer *C* (50 m*M* bis-Tris pH 6.0, 200 m*M* NaCl, 5 m*M* L-threonine, 3 m*M* dithiotreitol). The purity of the protein was analyzed by SDS–PAGE stained using PageBlue protein-staining solution (Fermentas). The peak fractions were pooled and concentrated using Amicon Ultra Centrifugal Filters (Millipore) with a molecular-weight cutoff of 10 000. The protein concentration was measured by UV absorption at 280 nm. The oligomeric state of the protein at room temperature was analyzed by static light scattering (SLS) using an ÄKTA Purifier (GE Healthcare) equipped with an analytical gel-filtration column (Superdex S75 10/300, GE Healthcare) and an SLS detector (Wyatt Technology miniDAWN Tristar) (Nettleship *et al.*, 2008). Purified protein which was not immediately used was aliquoted, flash-frozen in liquid nitrogen and stored at 193 K until further use.

2.3. Crystallization

Purified *Mtb*-AK-β at a concentration of 30 mg ml^{-1} in buffer *C* was used for crystallization experiments. All initial crystallization screenings were performed at the High Throughput Crystallization Facility at the EMBL Hamburg Outstation, which is equipped with a Hydra II Plus One crystallization robot (Mueller-Dieckmann, 2006). Crystallization experiments were carried out using the sitting-drop vapour-diffusion method in 96-well plates (Greiner) at 292 K. 300 nl protein solution and 300 nl precipitant solution were equilibrated against 50 µl reservoir solution. Several different crystal forms suitable for X-ray diffraction were found in the initial screens and no further optimization of the crystallization conditions was necessary.

2.3.1. Crystal form *A*. Several compact crystals were obtained from condition No. 3 of the Qiagen EasyXtal Classics Suite II (100 m*M* bis-Tris pH 5.5, 2 *M* ammonium sulfate). 3 d after setting up the experiment a thick precipitate appeared. As the crystals were formed and as they grew the precipitate gradually disappeared again. 10 d after set-up fully grown single crystals were observed with no or little precipitate still present (Fig. 3*a*). The final dimensions of the crystals were 50 × 50 × 70 µm. The same crystal form was also obtained from condition No. 6 of the Qiagen EasyXtal Classics Suite (100 m*M* Tris pH 8.5, 2 *M* ammonium sulfate).

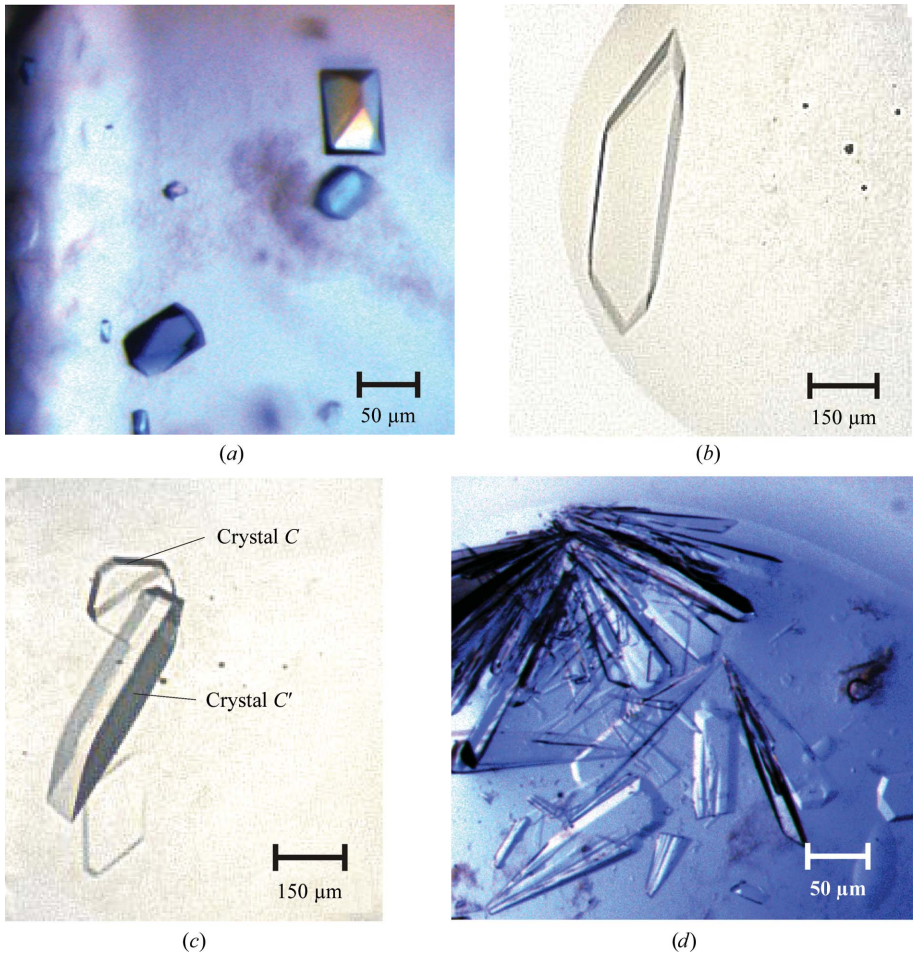

Figure 3
Crystals of *Mtb*-AK-β obtained by initial screening. (*a*) Primitive orthorhombic crystal form (crystal form *A*); (*b*) primitive tetragonal crystal form (crystal form *B*); (*c*) two related *I*-centred orthorhombic crystal forms (crystal forms *C* and *C*′); (*d*) *C*-centred monoclinic crystal form (crystal form *D*).

Table 1
Data-collection and processing statistics.

Values in parentheses are for the highest resolution shell.

Crystal form	*A*	*B*	*C*	*C′*	*D*
Wavelength (Å)	1.000	0.97622	1.000	1.000	1.000
Crystal-to-detector distance (mm)	160	260	160	220	250
Rotation range per image (°)	1.4	1.0	0.5	0.5	1.0
Total rotation range (°)	140	80	100	150	200
Exposure time per image (s)	15	10	10	6	10
Space group	$P2_12_12_1$	$P4_12_12$ or $P4_32_12$†	$I222$ or $I2_12_12_1$†	$I222$ or $I2_12_12_1$†	$C2$
Resolution range (Å)	99.0–1.62 (1.65–1.62)	99.0–2.92 (2.99–2.92)	99.0–1.73 (1.76–1.73)	99.0–2.43 (2.47–2.43)	99.0–2.86 (2.93–2.86)
Unit-cell parameters					
a (Å)	53.70	62.14	62.82	64.10	90.26
b (Å)	63.43	62.14	96.02	127.12	65.44
c (Å)	108.85	182.46	127.30	290.33	55.20
β (°)	90	90	90	90	106.28
Mosaicity (°)	0.24	1.19	0.78	0.70	0.80
Total no. of reflections	265591	49158	163438	255478	29395
Unique reflections	48641	8421	40507	45129	7224
Multiplicity	5.6 (4.7)	5.9 (6.1)	4.0 (4.0)	5.7 (5.3)	4.1 (3.9)
$\langle I/\sigma(I)\rangle$	21.8 (2.2)	11.1 (2.0)	14.3 (2.1)	10.6 (2.1)	11.3 (2.0)
Completeness (%)	99.9 (100)	99.8 (100)	99.9 (100)	99.6 (99.5)	100 (100)
$R_{\rm merge}$‡ (%)	7.5 (73.0)	14.3 (69.5)	9.0 (79.0)	15.0 (87.4)	11.9 (54.0)
$R_{\rm r.i.m.}$‡ (%)	8.3 (83.4)	15.7 (76.1)	10.4 (90.9)	16.6 (96.9)	13.7 (61.6)
$R_{\rm p.i.m.}$‡ (%)	3.4 (38.2)	6.4 (30.8)	5.1 (44.2)	7.0 (40.9)	6.7 (30.6)
Overall *B* factor from Wilson plot (Å^2)	21.8	62.8	20.9	45.3	57.5
Optical resolution (Å)	1.38	2.11	1.43	1.84	2.08
Matthews parameter (Å^3 Da^{-1})	2.40	4.55–2.28	2.48	2.55	2.02
Solvent content (%)	48.7	73.0–46.0	50.5	51.8	39.2
No. of molecules per asymmetric unit	2	1–2	2	6	2

† The final space-group assignment will have to await successful structure determination. ‡ The merging *R* factor $R_{\rm merge} = \sum_{hkl}\sum_i |I_i(hkl) - \langle I(hkl)\rangle|/\sum_{hkl}\sum_i I_i(hkl)$; the redundancy-independent merging *R* factor $R_{\rm r.i.m.} = \sum_{hkl}[N/(N-1)]^{1/2}\sum_i |I_i(hkl) - \langle I(hkl)\rangle|/\sum_{hkl}\sum_i I_i(hkl)$, where *N* is the number of times a given reflection *hkl* was observed; the precision-indicating merging *R* factor $R_{\rm p.i.m.} = \sum_{hkl}[1/(N-1)]^{1/2}\sum_i |I_i(hkl) - \langle I(hkl)\rangle|/\sum_{hkl}\sum_i I_i(hkl)$ (Weiss, 2001).

2.3.2. Crystal form *B*. A single crystal was grown from condition No. 48 of the Qiagen EasyXtal Classics Suite [200 m*M* bis-Tris propane pH 7.0, 15%(*w*/*v*) PEG 2000]. After 4–6 d the crystal reached its final dimensions of about 150 × 650 × 30 µm (Fig. 3*b*).

2.3.3. Crystal forms *C* and *C′*. Condition No. 73 of the Qiagen EasyXtal Classics Suite [500 m*M* NaCl, 100 m*M* sodium phosphate pH 7.0, 20%(*w*/*v*) PEG 4000] yielded four crystals (Fig. 3*c*). However, crystal growth only started about 20 d after setting up the experiment and was concluded 7 d later. Two thin crystals (form *C*) with a triangular shape with about 150 µm edge length and a thickness of about 20 µm appeared. One of these turned out to be two crystals grown together. A somewhat larger, more bulky looking single crystal (form *C′*) grew from the same drop to dimensions of about 360 × 300 × 80 µm.

2.3.4. Crystal form *D*. Crystals obtained from condition No. 92 of the Qiagen EasyXtal pHClear II Suite (1.5 *M* sodium malonate pH 7.0) exhibited a plate-like shape with dimensions of about 120 × 40 µm and only a few micrometres in thickness (Fig. 3*d*). Crystal growth started 13 d after setting up the experiment. The same crystal form was also obtained from condition No. 76 of the Qiagen EasyXtal PEGs Suite [200 m*M* calcium acetate, 20%(*w*/*v*) PEG 3350], albeit with a more compact crystal appearance.

2.4. Diffraction data collection and processing

Diffraction data collection was performed on beamline X12 at EMBL Hamburg. All diffraction experiments were carried out at 100 K in a nitrogen stream using single crystals. All crystals were cryoprotected using paraffin oil (Hampton Research) by adding 5 µl paraffin oil on top of the crystallization drop. The crystals were then picked up from the crystallization drop using a nylon loop, moved through the oil and directly frozen in the nitrogen stream. Single crystals of forms *A*, *C′* and *D* were mounted directly in the nitrogen stream on the beamline. During the attempt to mount the single form *B* crystal the crystal broke into pieces and only part of it was then used for the X-ray diffraction experiment. A crystal of form *C* had to be separated from a neighbouring crystal using a needle.

Indexing and integration of all data sets was performed using the program *DENZO* (Otwinowski & Minor, 1997) and was followed by scaling with *SCALEPACK* (Otwinowski & Minor, 1997). The space groups of the crystals were tentatively assigned based on scaling statistics and systematic absences using the program *POINTLESS* (Evans, 2006). The *R* factors $R_{\rm r.i.m.}$ (redundancy-independent merging *R* factor) and $R_{\rm p.i.m.}$ (precision-indicating merging *R* factor) (Weiss, 2001) were calculated using the program *RMERGE* (available from http://www.embl-hamburg.de/~msweiss/projects/msw_qual.html or from MSW upon request). All relevant data-collection and processing parameters are given in Table 1. Intensities were converted to structure-factor amplitudes using the program *TRUNCATE* (French & Wilson, 1978; Collaborative Computational Project, Number 4, 1994). The optical resolution of the data set and the data twinning were analyzed with *SFCHECK* (Vaguine *et al.*, 1999). The self-rotation function was computed using the program *MOLREP* (Vagin & Teplyakov, 1997; Collaborative Computational Project, Number 4, 1994) based on structure-factor amplitudes to a maximum resolution of 3.0 Å. Matthews parameters were determined using *MATTHEWS_COEF* (Matthews, 1968; Collaborative Computational Project, Number 4, 1994).

3. Results and discussion

The *Mtb* genome codes for a single monofunctional $\alpha_2\beta_2$-type aspartokinase. The genomic sequence coding for the *Mtb*-AK-β subunit was successfully cloned into the pETM-13 expression vector and strongly overexpressed in *E. coli*, resulting in about 20 mg pure protein per gram of wet cell pellet after the two-step chromatographic procedure. The optimal buffer composition for the purification

procedure was identified in a Thermofluor experiment (data not shown; Pantoliano *et al.*, 2001; Nettleship *et al.*, 2008). The purity of the sample was at least 95% as estimated by SDS–PAGE. A molecular weight of approximately 39 kDa was deduced from SLS experiments (data not shown), which is consistent with the value obtained by size-exclusion chromatography and indicates that in the presence of threonine *Mtb*-AK-β is a homodimer in solution. This finding is in agreement with the dimeric oligomerization state in the presence of feedback inhibitor found for the regulatory domains of other $\alpha_2\beta_2$-type aspartokinases (Yoshida *et al.*, 2007, 2009; C. Chang, H. Li, M. Gu & A. Joachimiak, unpublished work).

For *Mtb*-AK-β in the presence of the potential feedback inhibitor threonine four different crystallization conditions were identified which yielded crystals of sufficient size for X-ray diffraction experiments. All attempts to date to crystallize *Mtb*-AK-β in the absence of any feedback inhibitor or in the presence of the potential feedback inhibitor lysine were unsuccessful. Without Thr only conditions resulting in strong phase separation were obtained, which could not to date be optimized. Crystals from different crystallization conditions were tested for X-ray diffraction several weeks after set-up. For five crystals X-ray diffraction data could be collected to a resolution of better than 3 Å. The data-collection parameters and final statistics of the processed data are summarized in Table 1. No twinning was observed in any of the data sets.

3.1. Crystal form *A*

The crystal diffracted X-rays to 1.62 Å resolution, thus representing the highest resolution data available for crystals of *Mtb*-AK-β. The crystal belonged to the primitive orthorhombic space group $P2_12_12_1$, with unit-cell parameters a = 53.70, b = 63.43, c = 108.85 Å and an estimated two molecules in the asymmetric unit, corresponding to one complete regulatory domain. One independent peak which probably describes the twofold noncrystallographic symmetry of the AK-β dimer is clearly visible in the $\kappa = 180^\circ$ section in the self-rotation function (Fig. 4*a*).

3.2. Crystal form *B*

The piece broken off from a form *B* crystal exhibited diffraction to a resolution of at least 2.9 Å. The crystal belonged to the primitive tetragonal space group $P4_12_12$ or $P4_32_12$. The mosaicity of the crystal is rather high at 1.2°. A Matthews parameter (Matthews, 1968) calculation suggested the presence of one or two molecules per asymmetric unit. Calculation of the self-rotation function only shows peaks that can be ascribed to the crystallographic symmetry elements (Fig. 4*b*). Possible explanations could be that either only one molecule is present in the asymmetric unit or that the noncrystallographic twofold axis relating the two AK-β subunits is oriented parallel to a

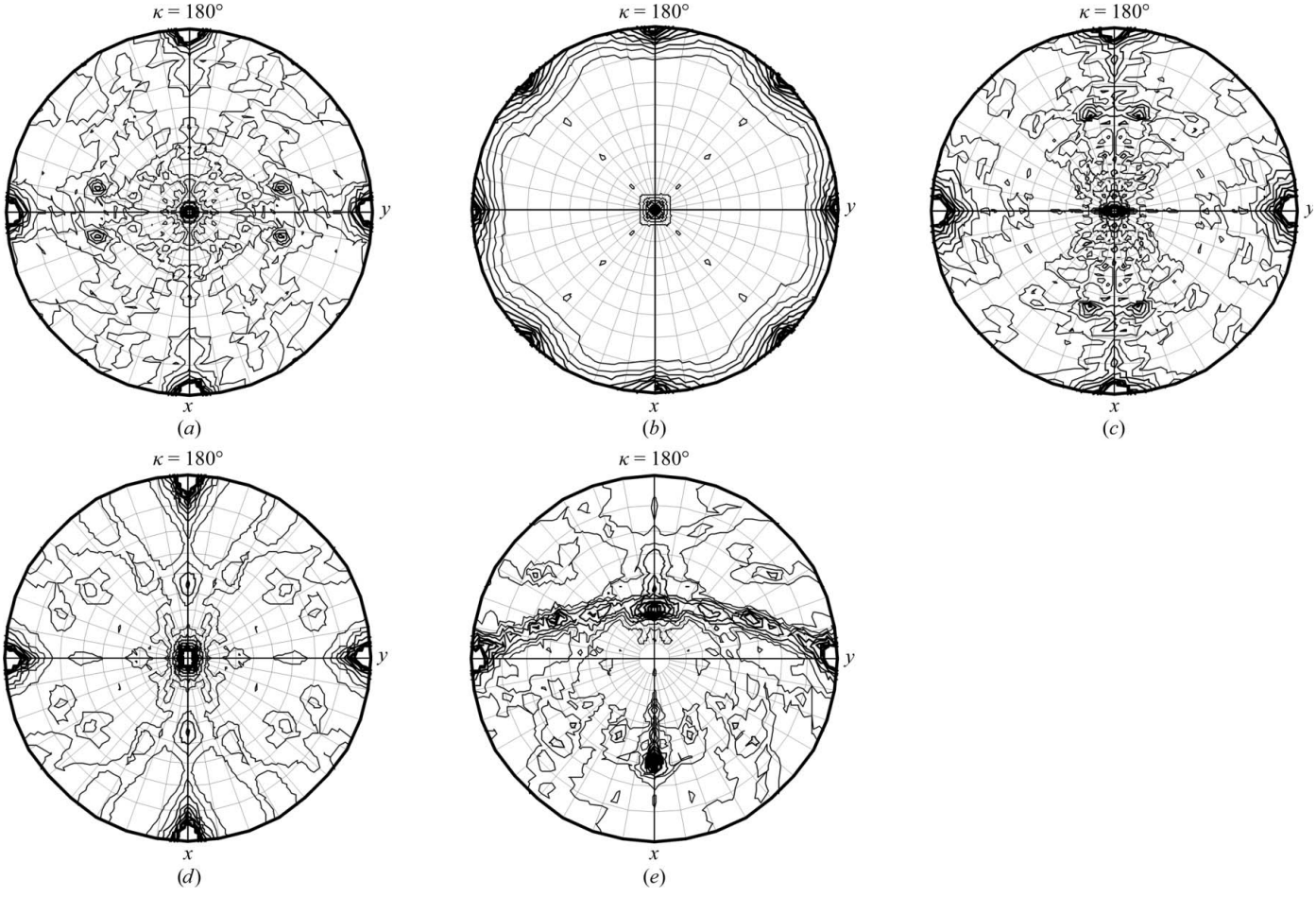

Figure 4
Self-rotation functions based on data collected from single crystals. The $\kappa = 180^\circ$ section indicating the relative position of twofold symmetry axes is shown. (*a*) Primitive orthorhombic crystal form (crystal form *A*); (*b*) primitive tetragonal crystal form (crystal form *B*); (*c*) *I*-centred orthorhombic crystal form (crystal form *C*; small unit cell); (*d*) *I*-centred orthorhombic crystal form (crystal form *C*′; large unit cell); (*e*) *C*-centred monoclinic crystal form (crystal form *D*).

crystallographic symmetry axis and is hence not visible as an individual peak in the $\kappa = 180^\circ$ section of the self-rotation function.

3.3. Crystal forms *C* and *C*′

The crystals grown from 500 m*M* NaCl, 100 m*M* sodium phosphate pH 7.0, 20%(*w*/*v*) PEG 4000 were found to belong to the *I*-centred orthorhombic space group *I*222 or $I2_12_12_1$. Interestingly, two related *I*-centred orthorhombic forms were obtained from the same crystallization drop. Crystal form *C* exhibits a small unit cell with unit-cell parameters $a = 62.81$, $b = 96.02$, $c = 127.28$ Å and two molecules in the asymmetric unit. The crystal examined showed anisotropic X-ray diffraction to a resolution of about 1.7 Å. The corresponding self-rotation function shows one independent peak indicating the position of the noncrystallographic twofold symmetry axis (Fig. 4*c*). Interestingly, the self-rotation function of the $\kappa = 180^\circ$ section looks similar to that from crystal form *A* (Fig. 4*a*) but is rotated by 90°, indicating a possible relationship between the two crystal forms. The crystal of form *C*′, which grew from the same crystallization drop, exhibits a larger unit cell with unit-cell parameters $a = 64.11$, $b = 127.12$, $c = 290.37$ Å and showed X-ray diffraction to beyond a resolution of 2.4 Å. The two forms *C* and *C*′ are obviously related in that the *a* and *c* axes of crystal form *C* are equivalent to the *a* and *b* axes of crystal form *C*′, respectively. The *c* axis of crystal from *C*′ is nearly three times the length of the *b* axis of crystal form *C*. This threefold elongation of the *c* axis of crystal form *C*′ compared with crystal form *C* is accompanied by a pseudo-translation with fractional coordinates (0.0, 0.0, 0.333). Considering the obvious relationship between the two forms *C* and *C*′ and the observation that the asymmetric unit of crystal form *C* contains two molecules of AK-β, the asymmetric unit of crystal form *C*′ is most likely to contain six molecules. In the $\kappa = 180^\circ$ section of the self-rotation function several weak peaks are present indicating the relative orientation of the noncrystallographic symmetry axes relating the AK-β dimers (Fig. 4*d*).

3.4. Crystal form *D*

A crystal of form *D* diffracted X-rays to a resolution of about 2.9 Å and belonged to the *C*-centred monoclinic space group *C*2. Calculation of the Matthews parameter indicated the likely presence of two molecules of AK-β in the asymmetric unit. Interestingly, the self-rotation function shows three independent peaks belonging to noncrystallographic symmetry elements (Fig. 4*e*). One peak is generated by the noncrystallographic twofold symmetry of the AK-β dimer. The remaining two peaks may be explained by the presence of pseudo-symmetry generated by the highly similar ACT1 and ACT2 domains. However, a final assignment of the peaks will have to await successful structure determination.

With sequence-identity values of *Mtb*-AK-β to AK-βs of known structure from *C. glutamicum*, *T. thermophilus* and *N. meningitides* of about 68, 37 and 38%, respectively, structure determination of all five crystal forms is currently being attempted by molecular replacement. Once determined, the *Mtb*-AK-β structure will represent the eighth structure of an enzyme belonging to the lysine-biosynthetic pathway in *Mtb*. Furthermore, having these five different crystal forms of *Mtb*-AK-β available will allow an in-depth analysis of possible conformational changes and the influence of different packing effects on the overall structure.

We would like to thank Dr L. Jeanne Perry (University of California at Los Angeles, USA) for providing genomic *Mtb* H37Rv DNA and Dr Arie Geerlof (Helmholtz-Zentrum München) for providing the *E. coli* BL21 Star (DE3) chaperone combination 2 cells and the pETM-13 vector. We also greatly acknowledge access to the synchrotron-radiation facility at the EMBL Outstation, DESY, Hamburg, Germany. Finally, we would like to thank the X-Mtb consortium (http://www.xmtb.org) for funding through BMBF/PTJ grant No. BIO/0312992A.

References

Black, S. & Wright, N. G. (1955). *J. Biol. Chem.* **213**, 27–38.
Chipman, D. M. & Shaanan, B. (2001). *Curr. Opin. Struct. Biol.* **11**, 694–700.
Cohen, G. N., Stanier, R. Y. & Le Bras, G. (1969). *J. Bacteriol.* **99**, 791–801.
Cole, S. T. *et al.* (1998). *Nature (London)*, **393**, 337–544.
Collaborative Computational Project, Number 4 (1994). *Acta Cryst.* D**50**, 760–763.
De Marco, A., Deuerling, E., Mogk, A., Tomoyasu, T. & Bukau, B. (2007). *BMC Biotechnol.* **7**, 32–40.
Evans, P. (2006). *Acta Cryst.* D**62**, 72–82.
Faehnle, C. R., Liu, X., Pavlovsky, A. & Viola, R. E. (2006). *Acta Cryst.* F**62**, 962–966.
French, S. & Wilson, K. (1978). *Acta Cryst.* A**34**, 517–525.
Gasteiger, E., Hoogland, C., Gattiker, A., Duvaud, S., Wilkins, M. R., Appel, R. D. & Bairoch, A. (2005). *The Proteomics Protocols Handbook*, edited by J. M. Walker, pp. 571–607. Totowa: Humana Press.
Hutton, C. A., Perugini, M. A. & Gerrard, J. A. (2007). *Mol. Biosyst.* **3**, 458–465.
Janowski, R., Kefala, G. & Weiss, M. S. (2010). *Acta Cryst.* D**66**, 61–72.
Kefala, G., Janowski, R., Panjikar, S., Mueller-Dieckmann, C. & Weiss, M. S. (2005). *Acta Cryst.* F**61**, 718–721.
Kefala, G., Perry, L. J. & Weiss, M. S. (2005). *Acta Cryst.* F**61**, 782–784.
Kefala, G. & Weiss, M. S. (2006). *Acta Cryst.* F**62**, 1116–1119.
Kefala, G. & Weiss, M. S. (2008). *Acta Cryst.* F**64**, 62.
Matthews, B. W. (1968). *J. Mol. Biol.* **33**, 491–497.
Mueller-Dieckmann, J. (2006). *Acta Cryst.* D**62**, 1446–1452.
Nettleship, J. E., Brown, J., Groves, M. R. & Geerlof, A. (2008). *Methods Mol. Biol.* **426**, 299–318.
Otwinowski, Z. & Minor, W. (1997). *Methods Enzymol.* **50**, 760–763.
Pantoliano, M. W., Petrella, E. C., Kwasnoski, J. D., Lobanov, V. S., Myslik, J., Graf, E., Carver, T., Asel, E., Springer, B. A., Lane, P. & Salemme, F. R. (2001). *J. Biomol. Screen.* **6**, 429–440.
Pavelka, M. S. & Jacobs, W. R. (1996). *J. Bacteriol.* **178**, 6496–6507.
Raviglione, M. C. & Smith, I. M. (2007). *N. Engl. J. Med.* **356**, 656–659.
Robin, A. Y., Cobessi, D., Curien, G., Robert-Genthon, M., Ferrer, J.-L. & Dumas, R. (2010). *J. Mol. Biol.* **399**, 283–293.
Schuldt, L., Weyand, S., Kefala, G. & Weiss, M. S. (2008). *Acta Cryst.* F**64**, 863–866.
Schuldt, L., Weyand, S., Kefala, G. & Weiss, M. S. (2009). *J. Mol. Biol.* **389**, 863–879.
Umbarger, H. E. (1978). *Annu. Rev. Biochem.* **47**, 532–606.
Usha, V., Dover, L. G., Roper, D. I., Fütterer, K. & Besra, G. S. (2009). *Acta Cryst.* D**65**, 383–387.
Vagin, A. & Teplyakov, A. (1997). *J. Appl. Cryst.* **30**, 1022–1025.
Vaguine, A. A., Richelle, J. & Wodak, S. J. (1999). *Acta Cryst.* D**55**, 191–205.
Vyas, R., Kumar, V., Panjikar, S., Karthikeyan, S., Kishan, K. V. R., Tewari, R. & Weiss, M. S. (2008). *Acta Cryst.* F**64**, 167–170.
Weiss, M. S. (2001). *J. Appl. Cryst.* **34**, 130–135.
Weyand, S., Kefala, G., Svergun, D. I. & Weiss, M. S. (2009). *J. Struct. Funct. Genomics*, **10**, 209–217.
Weyand, S., Kefala, G. & Weiss, M. S. (2006). *Acta Cryst.* F**62**, 794–797.
Weyand, S., Kefala, G. & Weiss, M. S. (2007). *J. Mol. Biol.* **367**, 825–838.
World Health Organization (2009). *Global Tuberculosis Control: Epidemiology, Strategy, Financing.* WHO/HTM/TB/2009.411. Geneva: World Health Organization.
Yoshida, A., Tomita, T., Kono, H., Fushinobu, S., Kuzuyama, T. & Nishiyama, M. (2009). *FEBS J.* **276**, 3124–3136.
Yoshida, A., Tomita, T., Kurihara, T., Fushinobu, S., Kuzuyama, T. & Nishiyama, M. (2007). *J. Mol. Biol.* **368**, 521–536.
Yoshida, A., Tomita, T., Kuzuyama, T. & Nishiyama, M. (2010). *J. Biol. Chem.* **285**, 27477–27486.